Article ID: 1006-8775(2017) 04-0450-12

# A PRINCIPAL MODE OF CIRCULATION COVARIATION BETWEEN THE NORTHERN AND SOUTHERN HEMISPHERES AND ITS ASSOCIATION WITH ENSO DURING BOREAL WINTER

TANG Wei-ya (唐卫亚), GUAN Zhao-yong (管兆勇), QIAN Dai-li (钱代丽)
(Key Laboratory of Meteorological Disaster, Ministry of Education (KLME) / Joint International Research Laboratory of Climate and Environment Change (ILCEC) / Collaborative Innovation Center on Forecast and Evaluation of Meteorological Disasters (CIC-FEMD), Nanjing University of Information Science & Technology, Nanjing 210044 China)

**Abstract:** By employing the singular value decomposition (SVD) analysis, we have investigated in the present paper the covariations between circulation changes in the Northern (NH) and Southern Hemispheres (SH) and their associations with ENSO by using the NCEP/NCAR reanalysis, the reconstructed monthly NOAA SST, and CMAP precipitation along with NOAA Climate Prediction Center (CPC) ENSO indices. A bi-hemispheric covariation mode (hereafter BHCM) is explored, which is well represented by the first mode of the SVD analysis of sea surface pressure anomaly (SLPA-SVD1). This SVD mode can explain 57.36% of the total covariance of SLPA. BHCM varies in time with a long-term trend and periodicities of 3—5 years. The long term trend revealed by SVD1 shows that the SLP increases in the equatorial central and eastern Pacific but decreases in the western Pacific and tropical Indian Ocean, which facilitates easterlies in the lower troposphere to be intensified and El Niño events to occur with lower frequency. The spatial pattern of the BHCM looks roughly symmetric about the equator in the tropics, whereas it is characterized by zonal disturbances in the mid-latitude of NH and is highly associated with AAO in the mid-latitude of SH. On inter-annual time scales, the BHCM is highly correlated with ENSO. The atmosphere in both the NH and SH responds to sea surface temperature anomalies in the equatorial region, while the contemporaneous circulation changes in the NH and SH in turn affect the occurrence of El Niño/La Niña. In boreal winter, significant temperature and precipitation anomalies associated with the BHCM are found worldwide. Specifically, in the positive phase of the BHCM, temperature and precipitation are anomalously low in eastern China and some other regions of East Asia. These results are helpful for us to better understand interactions between circulations in the NH and SH and the dynamical mechanisms behind these interactions.

**Key words:** Northern and Southern Hemispheres; circulation variations; covariation mode; climate anomaly; ENSO
**CLC number:** P434.3 **Document code:** A
doi: 10.16555/j.1006-8775.2017.04.010

## 1 INTRODUCTION

The Fifth Assessment Report of IPCC (Intergovernmental Panel on Climate Change) clearly states that global warming is an indisputable fact. Large amounts of observational and numerical modeling studies have shown that atmospheric green house gases have been increasing, surface temperature has warmed (Joshi et al.[1]), Arctic sea-ice has declined significantly (Zhang et al.[2]); the sea level is rising (Domingues et al.[3]), the number of extreme weather and climate events has been increasing, even the geographic pattern and intensity of droughts and floods have changed (IPCC[4]). Global warming has caused great attention and triggered more scientific interests in the study of global atmospheric circulation.

In recent decades, with increases in observations and the development of global models, more and more studies about global circulation have been conducted. These studies involve the global water and energy cycle (Chahine [5]; Soroochian et al.[6]), global circulation change and its regional response (Christy et al.[7]; Kusunoki et al. [8]), global climate system simulation (Giorgi [9]; Thompson and Pollard[10]; Chen and Fu[11]; Ju and Wang[12]), and hemispheric-scale atmospheric circulation and interactions (Findlater [13]; Carleton [14]; Zeng and Li[15]), and so on. Results of these studies have deepened our understanding of mechanisms behind climate changes and enhanced our capability to predict future climate. However, the global circulation changes are extremely complex, and our knowledge is far less than enough to fully understand these changes and the mechanisms behind.

**Received** 2016-04-13; **Revised** 2017-09-20; **Accepted** 2017-11-15
**Foundation item:** National Natural Science Foundation of China (41330425; 41175062)
**Biography:** TANG Wei-ya, Ph.D., Senior Engineer, primarily undertaking research on climate dynamics.
**Corresponding author:** GUAN Zhao-yong, e-mail: guanzy@nuist.edu.cn

Generally, the dominant components of large-scale atmospheric circulation in the Northern and Southern Hemispheres are almost independent of each other. Due to the asymmetric land-sea distribution and solar radiation between the two hemispheres, the perfect symmetric structure of the atmospheric circulation about the equator is not observed, and the ocean-atmosphere interaction results in extremely complex atmospheric circulation patterns in each hemisphere. The North Atlantic Oscillation (NAO) (Wallace [16]; Watanabe [17]), the Pacific Decadal Oscillation (PDO) (Mantua et al.[18]) and the Arctic Oscillation (AO) (Thompson and Wallace [19]) in the Northern Hemisphere (NH), the Antarctic Oscillation (AAO) (Gong and Wang[20]) in the Southern Hemisphere (SH), and some other teleconnection patterns (Wallace and Gutzler[21]; Hoskins et al.[22]; Shi and Zhu [23]) are examples of the complex circulation patterns in the two hemispheres. These teleconnections usually occur in the extratropics and are confined within their respective hemispheres, affecting global weather and climate variability.

However, significant interactions exist between the two hemispheres. ENSO (Cao et al.[24]; Liu et al.[25]), IHO (Interhemispheric Oscillation) (Guan and Yamagata [26]), the cross-equator flow (Wang and Li[27]) and related seasonal variation of Hadley Circulation actually lead to exchanges of atmospheric mass, energy, and momentum between the two hemispheres, inducing the redistributions of atmospheric mass and contemporaneous circulation changes in both hemispheres. Specifically, as one of the strong signals in the climate system, ENSO is highly associated with circulation anomalies in the SH and also affects circulation in the NH. Although there have existed many studies about the interaction between the two hemispheres, research about the contemporaneous changes in planetary circulations in the SH and NH are still limited. Is it possible to get a clear picture of the contemporaneous circulation variations in the Northern and Southern Hemispheres based on analysis of global scale changes in some basic atmospheric elements? In this study, we have revealed the contemporaneous circulation variations in the NH and SH by conducting the singular value decomposition (SVD) analysis of sea level pressure anomaly. Results of this study will deepen our understanding of the mechanism behind global circulation changes and ENSO impacts.

## 2 DATA AND METHODOLOGY

The data used in this study include (1) the NCAR/NCEP monthly mean reanalysis of sea level pressure, geopotential height, water vapor mixing ratio, wind fields, and temperature with a horizontal resolution of 2.5° × 2.5° in latitude and longitude (Kalnay et al.[28]), (2) the reconstructed NOAA sea surface temperature (SST) with the resolution of 2°× 2°, (3) the NOAA-CPC CMAP precipitation (Xie and Arkin[29]), (4) the Southern Oscillation (SO) index, and (5) Niño SST index over various regions, etc. All the above datasets cover the period of 1978—2014. Winter is defined to be December, January and February (DJF) in the NH. Wintertime average refers to the average over DJF. The Singular Value Decomposition (SVD) analysis, wavelet analysis, and correlation and regression analysis are implemented in this study.

## 3 CONTEMPORANEOUS CHANGES OF CIRCULATIONS IN THE NH AND SH

The atmospheric circulation variations in the NH and SH interact with each other though they are independent of each other. In order to reveal the contemporaneous circulation changes in the two hemispheres, the SVD analysis of SLPA (sea level pressure anomaly) has been conducted in this study. The SLPA to the north of 2.5° N for the NH winters of 1978/79—2013/14 is taken as the left field and the SLPA to the south of 2.5° S is taken as the right field for the SVD analysis. Statistics of the two leading SVD modes are given in Table 1. The two leading modes account for 57.36% and 21.80% of the total square of covariance, respectively. Their cumulative covariance proportion is up to 79.16% . These two modes correspond to the most significant contemporaneous SLP changes in the NH and SH during wintertime. Here we focus on the first leading mode (hereafter SVD1). The spatial distribution and temporal evolution of SVD1 are shown in Fig.1.

The contemporaneous changes of SLPA in the two hemispheres are roughly symmetric about the equator, particularly in the lower latitudes (Fig.1a and 1b). Apparently there exists a bi-hemisphere covariation mode (BHCM) between circulations in the two hemispheres. In the tropics, the SLPA is positive from the eastern Pacific to the east of the dateline. The two centers of positive SLPA are located near the equator and around (150° W, 15° S) respectively. On other longitudes in the tropics, the SLPA is negative. The center of negative SLPA is found over the Maritime Continent. Such an SLPA distribution tends to induce anomalous zonal winds, which are closely related to ENSO. For convenience, here we define the positive phase of BHCM if SLPA is positive in the east and negative in the west in the low-latitudes of the Indian-Pacific region, and the vice versa for the negative BHCM phase.

There are large differences in contemporaneous circulation variations in the mid- and high- latitudes between the two hemispheres. In the NH (Fig.1a), alternatively positive and negative SLPAs are found over the Caspian Sea-Aral Sea-Lake Baikal, Sakhalin-the Japanese archipelago, Northeast Pacific-west coast of North America and to the south of Hudson Bay, and the SLPA is relatively large over the Aral Sea-Lake Baikal region and Northeast Pacific-west

**Table 1**. Statistics of the two leading SVD modes of SLPA in the NH and SH.

| Statistics | SVD1 | SVD2 |
|---|---|---|
| Contribution to total covariance (%) | 57.36 | 21.80 |
| Cumulative of contributions to total covariance (%) | 57.36 | 79.16 |
| Correlations between the expansion coefficients | 0.90 | 0.63 |
| Explained left variance (%) | 17.49 | 24.57 |
| Explained right variance (%) | 24.50 | 13.61 |

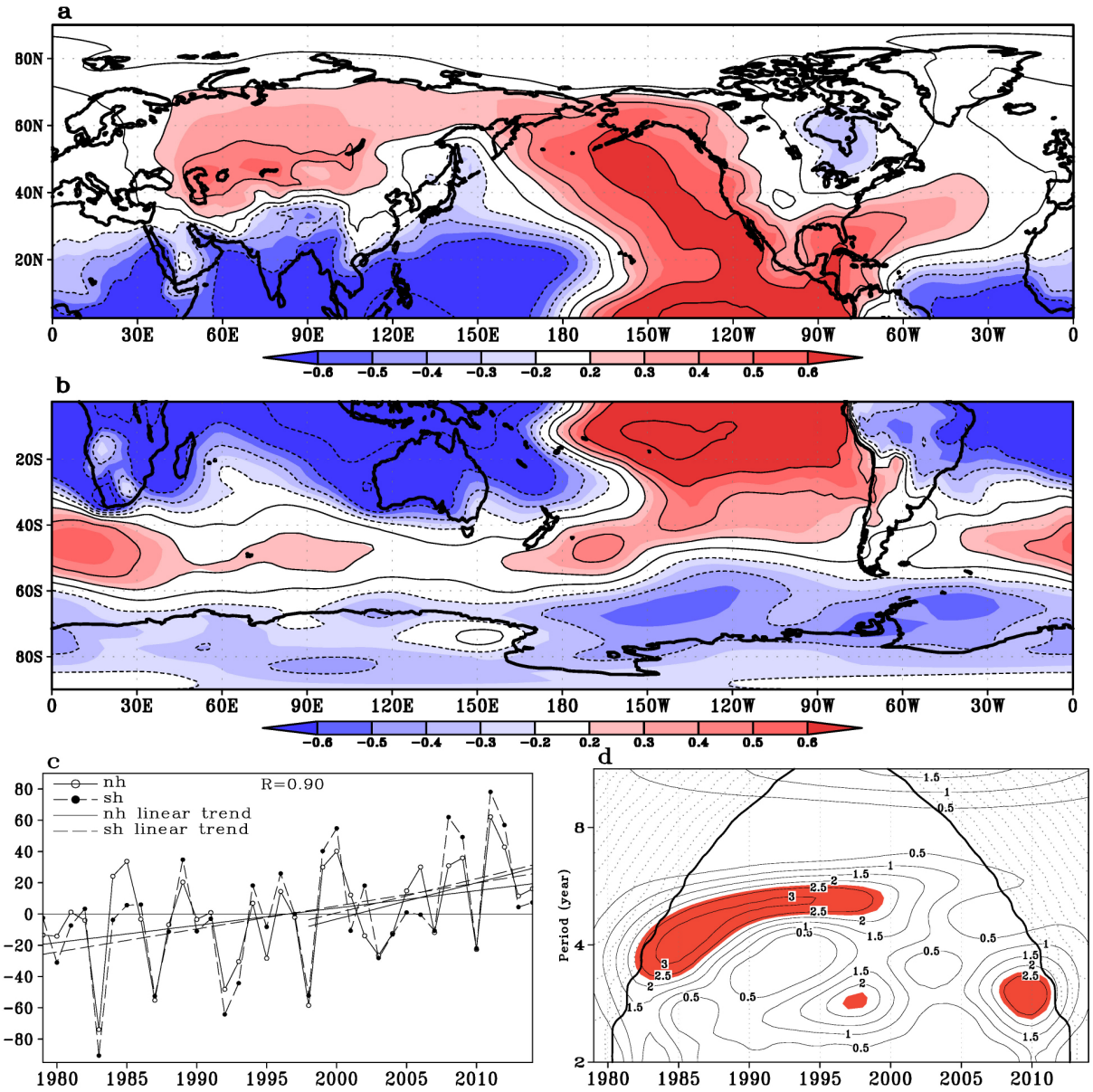


**Figure 1**. Heterogeneous correlations of SLPA for mode SVD1 in the NH (left field) (a) and SH (right field) (b), the corresponding time-series of coefficients along with their long-term trends (c), and the wavelet spectra of time-series of coefficients (d). The thresholds of correlation coefficients at the 90% and 95% confidence levels are 0.27 and 0.32 respectively. Solid and dashed lines in (c) are for the NH and SH respectively. Shaded areas in (d) indicate that the values are statistically significant at/above the 95% confidence level.

coast of North America region. In the meridional direction, SLPA in the inland region of mid-latitude is in opposite phase to that in low-latitude. In the mid- and high-latitude of the SH (Fig.1b), two zonal bands of SLPA in opposite phase are found, i.e., a positive SLPA band within 40 °S—60 °S coexists with a negative SLPA band in high-latitude. This pattern looks similar to the pattern of Antarctic Oscillation (AAO) (Gong and

Wang[20]; Thompson and Wallace[30]), and the simultaneous correlation of time-series of SVD1 coefficients with AAO index is 0.67. By comparing SLPA distributions in mid- and high- latitude of the two hemispheres as displayed in Fig.1a and 1b, we find that the zonal disturbance is more significant in the NH than in the SH, whereas the zonal symmetry of the disturbance is more distinct in the SH than in the NH. The difference in the SLPA pattern between the NH and SH is probably caused by difference in the ratio of land to ocean, while the fact that the NH winter is the SH summer may also contribute to this difference.

The correlation of the time-series of coefficients of the right field of SVD1 with that of the left field of is 0.90, indicating that SLPA changes in the NH and SH are well synergetic. Fig.1c shows that changes in SLPA are dominated by inter-annual variability in both hemispheres with major periods of 3−5a (Fig.1d), which is similar to the ENSO cycle with the periods of 3−7a.

Note that a long-term trend is found in the time series of the time coefficient of SVD1 in the most recent 30 years since 1978. Fig.1c indicates that the time coefficient is mostly positive since the early 21st century whereas it is mostly negative before that time, suggesting that the SLP has been decreasing during the NH wintertime in the recent 30a over the tropical Atlantic, Indian Ocean, western Pacific and areas near the Antarctica. In contract, the SLP has been increasing over the central-eastern Pacific, Caspian Sea-Aral Sea-Lake Baikal, northeastern Pacific and the west coast of North America. This trend leads to zonal wind changes near ocean surface above the equator, where the easterly has intensified anomalously over the central-eastern Pacific while the westerly has abnormally weakened since 1998. Such changes in circulation are unfavorable for the development of strong El Niño. McPhaden et al. proposed that in the recent 10a since the beginning of the 21st century, the frequency of eastern Pacific type El Niño event has been decreasing while that of central-Pacific type El Niño event has been increasing [31-32], which is consistent with the SLP changing trend revealed by the present study. On the other hand, SLP anomalies shown in SVD1 are very small in the high-latitude of NH, suggesting that changes in atmospheric circulation in the NH high-latitude contribute little to the contemporaneous changes of circulation in the two hemispheres.

The similarity between SLPA-SVD1 and SLPA is analyzed to further reveal the specific characteristics of the BHCM. Spatial pattern correlation between SLPA and the left field of SVD1 in the NH is calculated to determine those years when the SLPA pattern is similar to that of SVD1. A similar analysis is also performed for the SH. Results are presented in Fig.2, which shows that the inter-annual variability of similarity coefficients (pattern correlation coefficients) between SLPA-SVD1 and SLPA is consistent with that of the time-series of coefficients of SVD1 in both the NH and SH. The correlation coefficients between the time series of similarity coefficients and that of the SVD1 coefficients are greater than 0.94 in both the NH and SH. This result again indicates that, to a large degree, SLPA in the two hemispheres change contemporaneously. Table 2 lists the years when the spatial pattern of SLPA is similar to that of SLPA-SVD1. Note that the dominant features of spatial distribution of SLP anomalies in these years are exactly the same as that shown in Fig.1a and 1b. Meanwhile, most of these years are ENSO years.

## 4 VERTICAL STRUCTURE OF THE LEADING MODES

The horizontal distribution of the contemporaneous SLP changes in the NH and SH has been discussed above. However, changes in SLP are actually the response of the atmosphere to abnormal thermal forcing on the surface atmosphere and circulation changes in the whole troposphere. Changes in the circulation above the earth surface in association with SVD1 are not clear yet. In the following work, global wind anomalies (Fig. 3) are obtained by regressing them onto the time series of coefficients of SLPA-SVD1.

In the positive BHCM phase, lower-level easterly disturbances (Fig.3c) are accompanied by mid- and upper-level (above 500hPa) westerly disturbances (Fig. 3a and 3b) over the equatorial Pacific (Fig.3); whereas

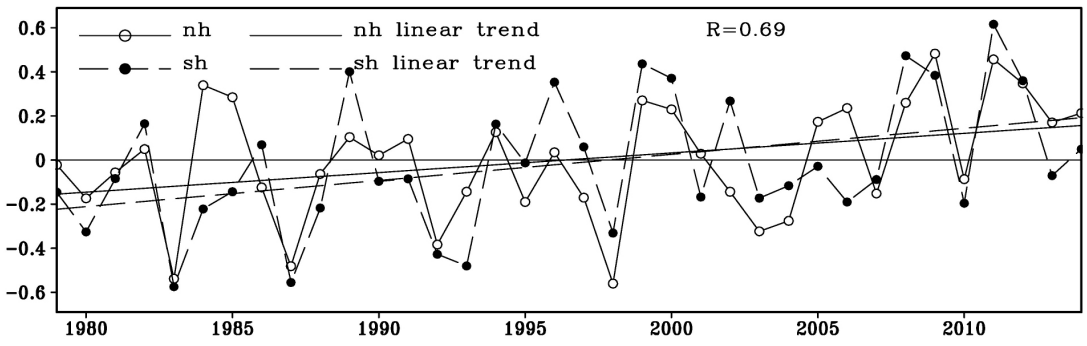


**Figure 2**. Time series of similarity coefficients (pattern correlations) between SLPA and SLPA-SVD1. The solid and dashed curves (straight lines) are for variations (the long-term trends) in the NH and SH, respectively.

**Table 2**. The years for which SLPA and SLPA-SVD1 have similar spatial patterns.

| SLPA pattern in the low-latitudes | Years with similar patterns of SLPA and SLPA-SVD1 | | | | | | |
|---|---|---|---|---|---|---|---|
| Positive in the east and negative in the west (positive phase) | 1984/85 | 1998/99 | 1999/00 | 2007/08 | 2008/09 | 2010/11 | 2011/12 |
| Negative in the east and positive in the west (negative phase) | 1982/83 | 1986/87 | 1991/92 | 1992/93 | 1994/95 | 1997/98 | 2009/10 |

over the Indian Ocean, westerly disturbances occur in the mid- and lower-level while easterly disturbances occur at the upper-levels in the troposphere. Easterly and westerly winds converge in the lower troposphere but diverge in the upper troposphere above the Maritime Continent, which actually depicts the ascending branch of the Walker circulation and indicates strong interaction between equatorial Pacific and Indian Ocean through the circulation anomaly (Wu and Meng [33]; Alexader et al.[34]) .

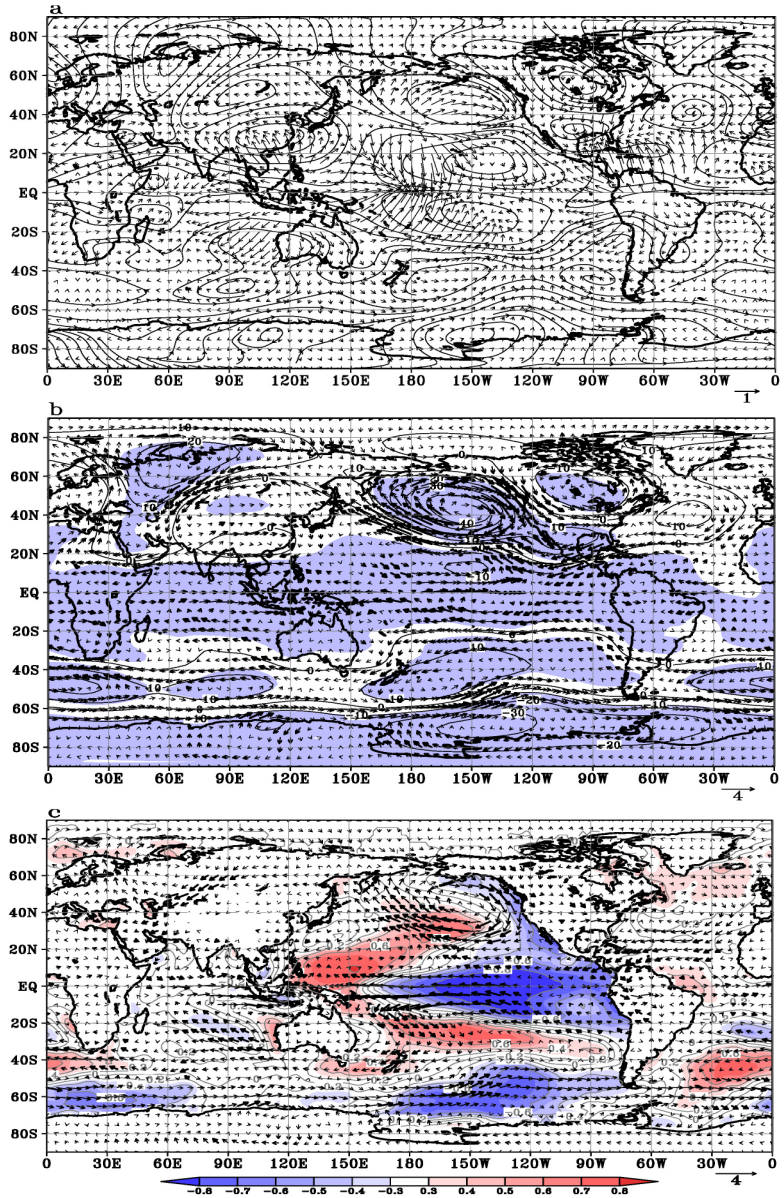


**Figure 3**. Regressions of wind and geopotential height anomalies against the time series of coefficients of SLPA-SVD1, and the spatial pattern of correlation between the time series of coefficients and global SSTA. Shown in (a) are rotational (streamlines, m·s$^{-1}$) and divergent (arrows, m·s$^{-1}$) wind components at 200hPa whereas in (b) are the anomalous winds (arrows, m·s$^{-1}$) and geopotential height (gpm) at 500hPa. The shaded areas indicate the values are statistically significant at/above 95% confidence level with F-test. Shown in (c) are the anomalous winds (arrows, m·s$^{-1}$) at 850hPa and the spatial pattern of correlations of time series of coefficients of SVD1 with SSTA (shaded). Shaded areas indicate the correlation coefficients are statistically significant at/above 90% confidence level. The bold arrows denote the values that are significant at/above 95% confidence level using an F-test.

Anomalous circulations at different levels in the troposphere all demonstrate a spatial structure that is roughly symmetric about the equator, particularly in the mid- and low-latitude. Over the Pacific region nearby the equator, a pair of abnormal circulation systems that are roughly symmetric about the equator but in opposite phase in the lower and upper troposphere can be found, i.e., anomalous anti-cyclonic circulation in the lower troposphere is accompanied by anomalous cyclonic circulation in the upper troposphere. The intensity of the anomaly increases with height. There exists an abnormal anti-cyclonic circulation with equivalent barotropic structure in mid- and high- latitudes above both the North and South Pacific. The center of the anti-cyclonic circulation over the North Pacific is located to the south of the Aleutian Islands, and the one over the South Pacific is located to the east of New Zealand. In the Asia-Australia region along 110°E , abnormal cyclonic-anticyclonic-cyclonic circulations alternatively exhibit pole-ward from the equator below 500hPa. In the upper troposphere nearby the Maritime Continent (Fig.3a), the cyclonic circulations that are roughly symmetric about the equator are not observed while easterlies develop above the equator. The anomalous circulations in extra-tropical regions look to be equivalent barotropic. In North and South America, there also have circulations that are symmetric about the equator in the mid- and lower-troposphere, but the circulations in the upper troposphere appear as easterly wave disturbances at 200hPa.

There are large differences in the mid- and high-latitude circulation anomalies between the NH and SH (Fig.3). Intensity of circulation anomalies in the NH looks to be stronger than that in the SH. In the NH, distinct zonal disturbances are observed; cyclonic and anticyclonic circulation anomalies distribute alternatively from northern Europe, the Urals, Siberia, northern Pacific to North America and North Atlantic in a wavy pattern with an equivalent barotropic vertical structure. The PNA (Pacific-North America) wave train (Wallace and Gutzler [21]) lies from the central-eastern Pacific to northern Pacific, North America and Gulf of Mexico. In the SH, the PSA (Pacific-South America) wave train (Carleton[14]) appears in the southern Atlantic and Pacific. The dominant mode of circulation anomaly in the mid- and high-latitude of SH is characterized by an annular structure, with anomalously low pressure perturbation in the polar region and high pressure perturbation in the surrounding ring.

The regression of vertical circulation against the time-series of coefficients of SLPA-SVD1 depicts the significant Walker Circulation above the equator (Fig. 4a). The ascending branch of the Walker Circulation is located over Kalimantan and the ocean to its east, while the two descending branches are located at the central-western Indian Ocean and central-eastern Pacific respectively. A strong vertical circulation is found from equatorial eastern Pacific to equatorial Atlantic and West Africa, with the ascending branch located at Amazon and the equatorial Atlantic, and the descending branch located over the Pacific. These circulation anomalies lead to higher SLPA over the central-eastern Pacific and lower SLPA over the western Pacific and eastern Indian Ocean. The lower level easterlies over the central-eastern Pacific subsequently intensify.

The vertical structure of meridional circulation near the ascending and descending branches of the Walker Circulation is distinctly different from the well-known classic three circulation cells. Looking at the meridional circulation along 110° E (Fig.4b), the three circulation cells can be found in the NH while only one exists in the SH. The air rises at the equator, flows northward and southward at around 200hPa, and sinks to the surface at 20° S—30° S and 20° N—30° N respectively. The vertical circulation at 30°N—45°N is different from that of the classic Ferrel cell in that its ascending branch is located at relatively lower latitudes and the air sinks in higher latitudes, which actually weakens the Ferrel cell. It is found that the abnormal circulation cell in the polar region in the NH shifts southward as compared with the classic polar cell. The vertical cross section of the meridional circulation along 150° W (Fig. 4c) presents three abnormal cells in both the NH and SH. The three abnormal cells in the NH produce prevailing air movements in opposite directions to that associated with the classic three cells. The two ascending branches of the abnormal cells are located near 15 °N and 80 °N, where the air rises to the upper level and flows northward and southward respectively, eventually sinks at the equator and around 45 °N. These abnormal circulations weaken the seasonal mean vertical circulation in the NH during wintertime. In the SH, two meridional cells can be found from 70 °S to the equator, with the centers located at 60 °S and 15° S respectively. The two cells converge at 40 °S and the convergence reaches up to 300hPa. An abnormal circulation, centered at 75 °S , appears in the high-latitude of SH.

## 5 RELATION BETWEEN BHCM AND ENSO

ENSO is an ocean-atmosphere coupling phenomenon that occurs in the tropics. It can be explained by the delayed oscillator theory (Suarez and Schopf[35]) or recharge oscillator theory (charge-discharge of ocean heat content) (Jin[36]). The atmosphere responds to SST anomalies in the equatorial region through the Gill-type mechanism (Gill[37]). Table 3 lists the correlation coefficients between various ENSO indices and time-series of SVD1 coefficients. It shows clearly that the time-series of coefficients of SLPA-SVD1 is highly correlated with monthly Niño indices and SO index (the correlation is statistically significant at 99.9% confidence level). The highest simultaneous correlation

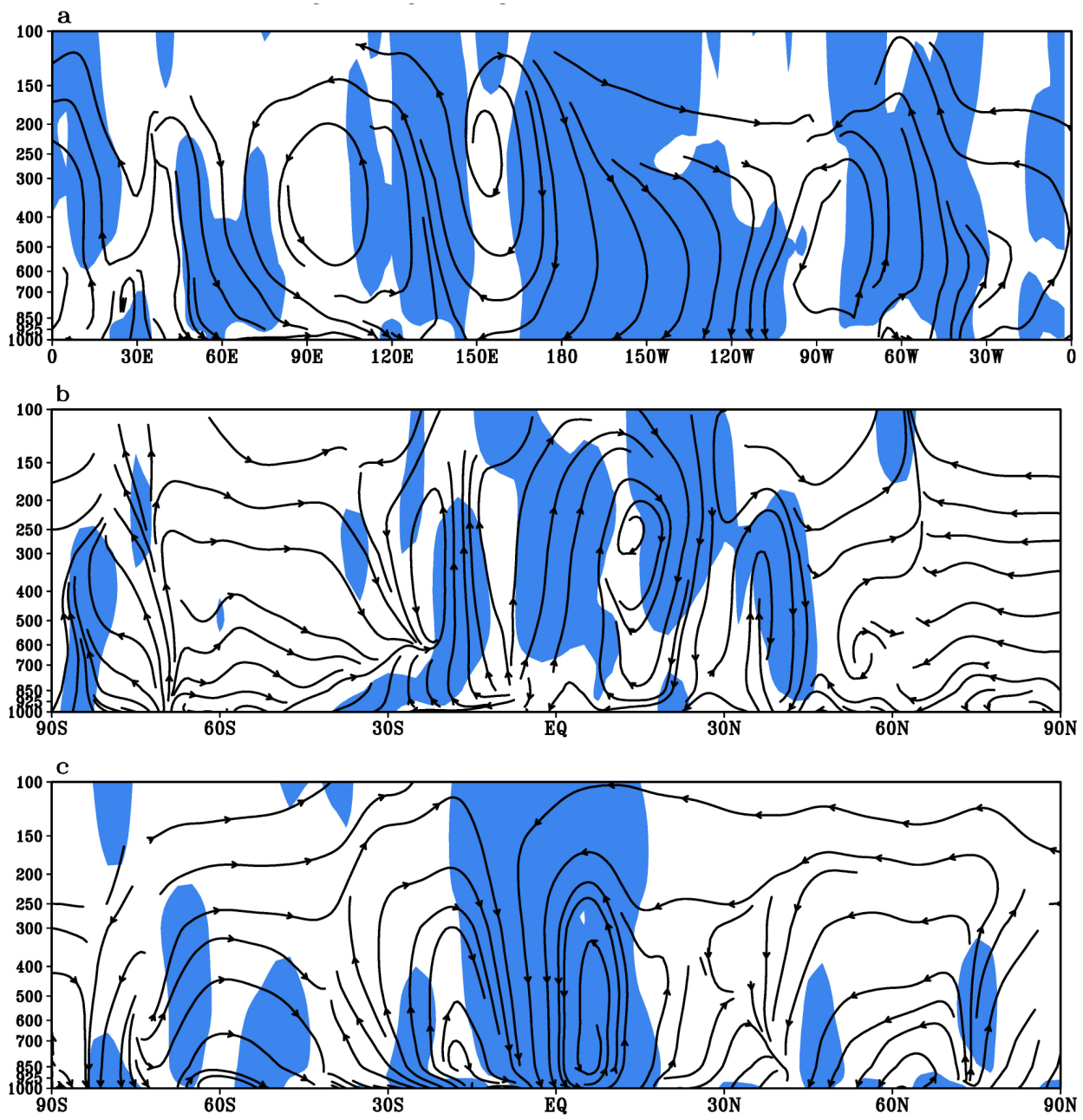


**Figure 4**. Regression of vertical circulations against time-series of coefficients of SLPA-SVD1 at (a) EQ, (b) 110°E, and (c) 150°W, respectively. The shaded areas indicate that regressed vertical velocity is statistically significant at/above 95% confidence level using an F-test.

of up to 0.86 is found between Niño3.4 index and the time-series of coefficients of SLPA-SVD1. Note that SVD1 is highly correlated with Niño that leads by 7 months or lags by 4 months (the correlation is significant at 95% confidence level). Meanwhile, the contemporary correlation coefficient between SVD1 and SO index is above 0.82, while the coefficient is 0.4 with SO leading by 7 months and 0.72 with SO lagging by 2 months. The correlation rapidly decreases since then, suggesting that ENSO has great impacts on contemporary circulation variations in the two hemispheres. The lagged correlation implies that the contemporary circulation changes in the two hemispheres will in turn affect ENSO.

In order to perceptively understand the relation between BHCM and ENSO, we present the spatial pattern of correlation coefficient between time-series of SVD1 coefficients and SSTA (Fig.3c). It reveals a La Niña pattern-like SST distribution associated with mega-ENSO events in the tropical Pacific (Wang et al.[38]). This further demonstrates the close relationship between BHCM and ENSO. Looking at Fig.1a, 1b, Fig.3 and Fig.4 together, it is readily apparent that the abnormal circulations symmetric about the equator in the tropical Pacific are exactly the atmospheric response to SSTA (Gill [37]), while the PNA pattern is a result of spherical

**Table 3**. Correlation coefficients between the time-series of coefficients of SLPA-SVD1 and ENSO indices. Asterisks and triangles denote the values statistically significant at/above 95% ($|r|_{\alpha=0.05}=0.32$) and 99.9% ($|r|_{\alpha=0.001}=0.51$) confidence levels, respectively.

| Leading/lagging (month) | Niño1+2 | Niño3 | Niño3.4 | Niño4 | SO |
|---|---|---|---|---|---|
| −8 | −0.01 | −0.02 | −0.18 | −0.22 | 0.26 |
| −7 | −0.10 | −0.25 | −0.37* | −0.38* | 0.40* |
| −6 | −0.16 | −0.43* | −0.57Δ | −0.49* | 0.36* |
| −5 | −0.23 | −0.52Δ | −0.62Δ | −0.53Δ | 0.51Δ |
| −4 | −0.38* | −0.60Δ | −0.68Δ | −0.59Δ | 0.69Δ |
| −3 | −0.54Δ | −0.71Δ | −0.74Δ | −0.69Δ | 0.74Δ |
| −2 | −0.64Δ | −0.76Δ | −0.78Δ | −0.71Δ | 0.72Δ |
| −1 | −0.70Δ | −0.80Δ | −0.82Δ | −0.70Δ | 0.83Δ |
| 0 | −0.70Δ | −0.86Δ | −0.89Δ | −0.77Δ | 0.90Δ |
| 1 | −0.65Δ | −0.82Δ | −0.89Δ | −0.76Δ | 0.82Δ |
| 2 | −0.56Δ | −0.69Δ | −0.81Δ | −0.62Δ | 0.72Δ |
| 3 | −0.50* | −0.52Δ | −0.61Δ | −0.54Δ | 0.06 |
| 4 | −0.40* | −0.32* | −0.36* | −0.40* | 0.18 |
| 5 | −0.30 | −0.19 | −0.16 | −0.23 | 0.19 |
| 6 | −0.24 | −0.13 | −0.04 | −0.07 | 0.03 |

Rossby wave propagation excited by the abnormal vorticity in the middle and upper troposphere in response to the tropical SSTA forcing (Wallace and Gutzler[21]; Hoskins and Karoly[39].

## 6 GLOBAL CLIMATE ANOMALY

### 6.1 *Relationship between global climate anomaly and BHCM*

The contemporary circulation changes in the SH and NH are closely related to climate anomalies at various regions worldwide. Here we analyze the correlations between the time coefficients of SLPA-SVD1 and global temperature and precipitation. The atmospheric moisture flux transport regressed against the time-series of coefficients of SLPA-SVD1 is also exploited to explore the effects of SLPA-SVD1 on global temperature and precipitation.

There are significant global anomalies of precipitation in association with BHCM. The correlation coefficients between precipitation and time-series of coefficients of SLPA-SVD1 demonstrate a spatial pattern that is roughly symmetric about the equator in lower latitudes (Fig.5). Significant correlations are found over the tropics and lower latitudes. The BHCM impact on precipitation looks similar to the well-known simultaneous effects of ENSO. Note that positive correlations are found over the Maritime Continent while negative correlations mainly occur in eastern China, implying that precipitation in these areas is greatly affected. In the positive phase of BHCM, the Maritime Continent experiences more wintertime precipitation, whereas eastern China, the coastal region of southeastern China, and southern US have less precipitation (Gong and Wang [40]). The regressed circulation (Fig.3 and Fig.4) indicates that in the positive phase of BHCM, surface pressure is abnormally high in the central-eastern Pacific with descending flows aloft, leading to less than normal precipitation there. In contrast, surface pressure is anomalously low in the Maritime Continent, where anomalous surface convergence of winds and ascending motions result in more precipitation (Lu et al.[41]). Under the influence of convective activities near the Maritime Continent, precipitation decreases in Yangtze-Huaihe River valley in China (Huang and Sun [42]). Precipitation also decreases in North America due to the effects of the PNA teleconnection.

The pattern of correlations between time-series of SVD1 coefficients and temperature anomalies suggests that the BHCM impact on temperature is similar to simultaneous ENSO influence on temperature in low-latitude. However, the correlation is in opposite sign to the results of Kiladis and Diaz in the southeastern part of the Maritime Continent and over the ocean to the east of Australia [43]. Again, areas of significant correlation are roughly symmetric about the equator. In addition, significant correlations also appear over zonally-extending areas in the high latitudes of both hemispheres. Areas of positive BHCM-precipitation correlation corresponds to areas of positive BHCM-temperature correlation over low-latitude ocean, i.e., anomalously more precipitation coexists with higher than normal temperature. The situation is contrary over the land, where anomalously more precipitation often corresponds to lower than normal temperature. In the positive phase of BHCM, positive temperature anomaly occurs over the eastern Maritime Continent while negative temperature anomaly appears in the central-eastern Pacific and the northern region of South America. In China, temperature is higher than normal in southwestern China but lower than normal in eastern China. A possible reason is that, the air rises over the Maritime Continent and sinks over

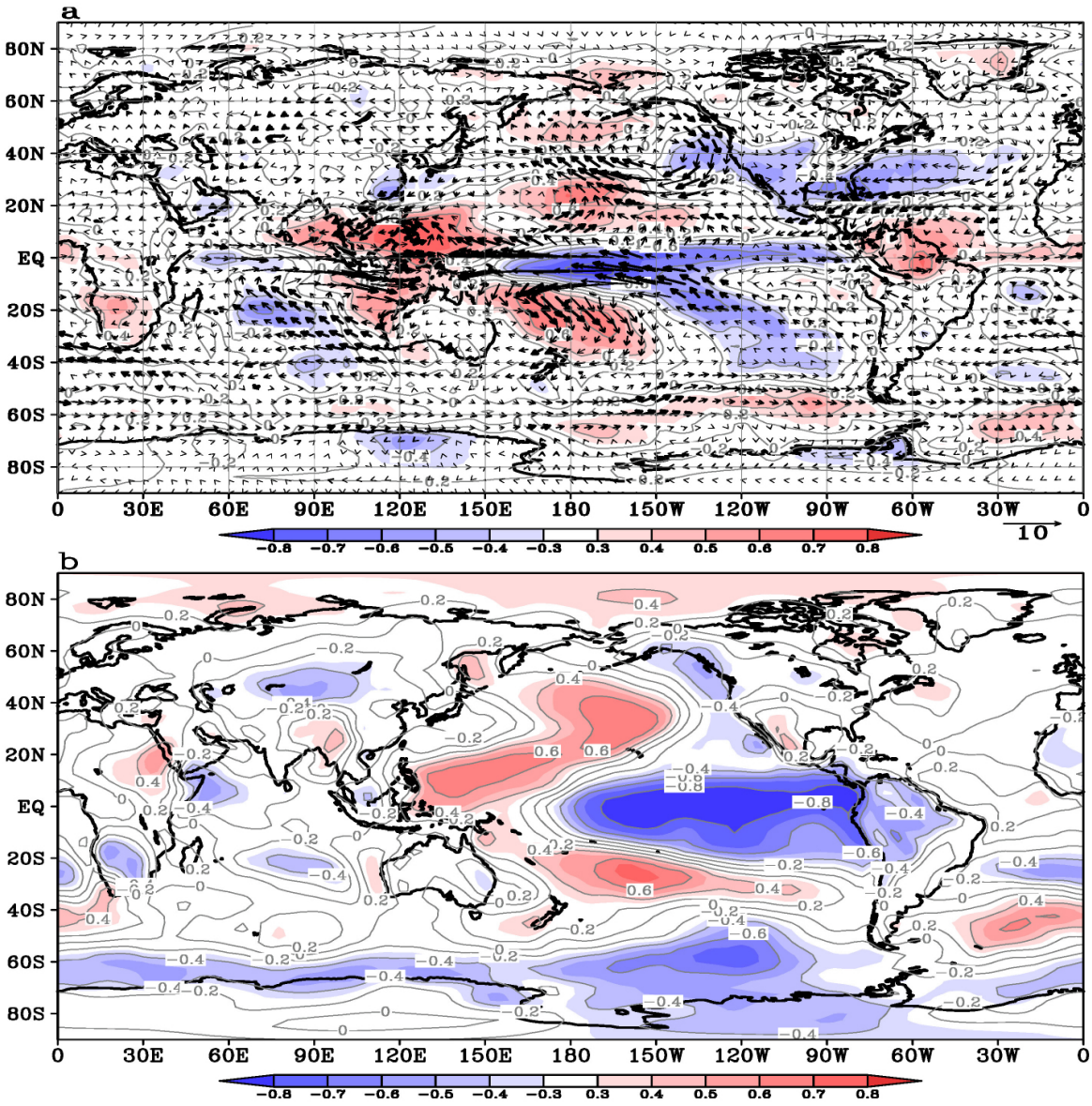


**Figure 5**. Correlation coefficient (shaded contours) between precipitation and time-series of coefficients of SLPA-SVD1, and regressed atmospheric moisture transport as obtained by integrating them vertically from 1,000 hPa up to 300 hPa against the time-series of coefficients of SLPA-SVD1 (arrows, in kg·(m·s)$^{-1}$ with bold arrows for the regressed moisture transport significant at/above 95% confidence level using an F-test (a), and correlation coefficients between temperature and the time-series of coefficients of SLPA-SVD1 (shaded contours) (b). The correlation coefficient thresholds for 90% and 95% confidence levels are 0.27 and 0.32 respectively.

the land (Fig.4b), inducing diabatic cooling in eastern China due to less cloud there in boreal winter.

6.2 *The slowdown in global warming and BHCM*

The time series of global mean temperature have shown that the global mean temperature reached its highest value in 1998. The global warming trend in the most recent 15 years is in sharp contrast to that in the previous 20 years before 1998. Since 1998, the rate of global warming has slowed down and the frequency of El Niño occurrence has decreased. As stated previously, the long-term trend of SVD1 reflects the fact that SLP has increased over the equatorial eastern Pacific but decreased in other tropical areas, which leads to abnormal pressure gradient changes in the tropics. As a result, the lower level easterlies have anomalously intensified since 1998. Differences in multi-year average wintertime surface temperature and pressure between 2000/01—2013/14 and 1978/79—1994/95 (Fig.6) also show that the east-to-west pressure gradient force has increased after 1998, accompanied with the intensified easterlies in the tropical Pacific (Fig.6a). SST decreases in the eastern Pacific and increases in the western Pacific correspondingly (Fig.6b).

## 7 CONCLUSIONS AND DISCUSSION

In the present paper we have employed the SVD

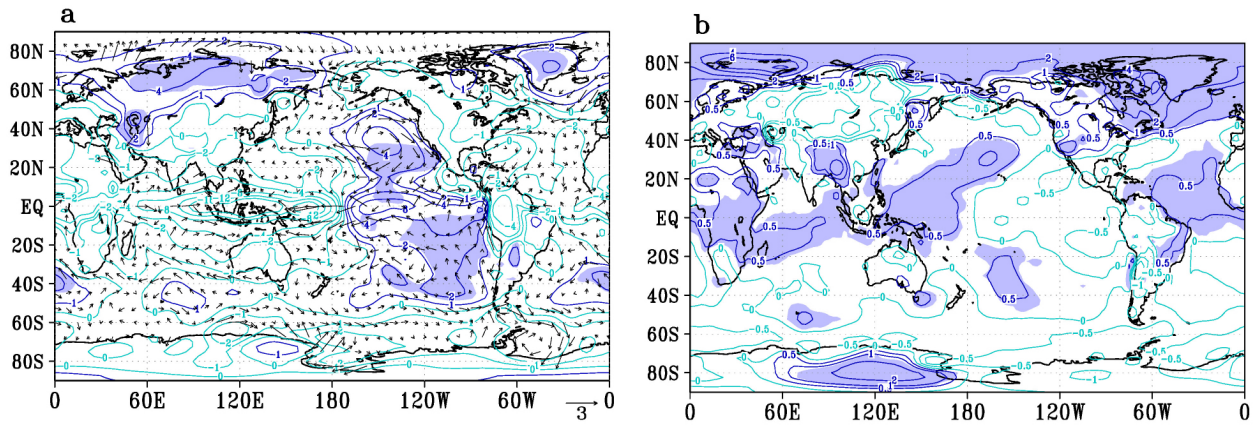


**Figure 6**. Differences in the multi-year average wintertime between 2000—2013 and 1978—1994, (a) sea level pressure SLP (contour, unit: hPa) and (b) surface temperature (contour, unit: ℃). Differences in surface wind fields are overlapped with that of SLP (arrows, unit: $m \cdot s^{-1}$). The shaded areas indicate the difference is significant at/above 95% confidence level using a *t*-test.

method to investigate the contemporaneous wintertime SLP change mode, i.e. BHCM, for the NH and SH. The spatial-temporal features of the BHCM mode and its relation to ENSO have been discussed. Major conclusions are as follows.

There exists a BHCM mode as revealed in SLPA, which is roughly symmetric about the equator in the tropics. Associated with the BHCM mode, zonal disturbance is distinct in the mid-latitude of NH; in the mid-latitude of SH, the BHCM mode is closely related to AAO. This mode can explain 57.36% of the total covariance of SLPA in the NH and SH.

The BHCM mode demonstrates a significant long-term trend, which is possibly associated with the slowdown of global warming. This long-term trend can lead to changes in zonal winds over the equatorial region and affect ENSO. Since 1998, the decrease in the frequency of El Niño event probably is also related to the long-term trend of BHCM.

The BHCM mode also has a clear cycle of 3—5 years. This cycle is closely related to ENSO and particularly the mega-ENSO (Wang et al. [38]) that is proposed recently. On one hand, the atmosphere responds to equatorial SSTA forcing on inter-annual time scale; on the other hand, contemporaneous circulation changes in the NH and SH can jointly affect El Niño /La Niña through the ocean-atmosphere interaction in the tropics.

Global temperature and precipitation anomalies during wintertime are closely linked with the BHCM mode of SLPA. In the positive phase of BHCM, abnormally high temperature and more precipitation occur over the Maritime Continent. However, precipitation is less than normal in eastern China and other regions of East Asia, where temperature remains normal or lower than normal. North America is under the influence of PNA teleconnection with less precipitation and higher temperature. There are some differences in the areas with significant changes due to the BHCM influence as compared with the contemporaneous influence of ENSO.

It is worth noting that if different ENSO indices are used to calculate the correlation coefficients with SLPA, the spatial pattern of the correlation coefficients is similar to the spatial distribution of SVD1 to a certain degree. However, the BHCM can reflect the contemporaneous circulation changes in the NH and SH. Table 3 indicates that the lagged correlation between the time-series of coefficients of SLPA-SVD1 and ENSO indices ranges between 0.4—0.8, while the contemporaneous correlation is within 0.7—0.9. This result implies that 20%—60% of the variance cannot be explained by each other. Even if ENSO does not occur, somehow the principal mode of contemporaneous circulation changes in the two hemispheres still exists. Meanwhile, note that there is a strong relationship between the BHCM mode and AAO, suggesting that the BHCM mode does not solely represent changes related to ENSO. We will further discuss this issue in another work.

In addition, it should be pointed out that the BHCM mode only reveals the contemporaneous circulation changes in the NH and SH and their relation to ENSO. However, it is still not clear about the anomalous circulations that are related to ENSO but do not change contemporaneously in the NH and SH. Furthermore, model simulations need to be analyzed to determine whether GCMs can successfully simulate the BHCM mode. This will be our future research topic.

***Acknowledgement***: We appreciate the reviewers for their constructive comments and suggestions. We thank the Data Center of Nanjing University of Information Science & technology for the data services. The global reconstructed SST data is provided by NOAA Earth System Research Laboratory (http://www.esrl.noaa.gov). NOAA Climate Prediction Center provides CMAP precipitation, SO indices, and Niño indices (http://www.cpc.ncep. noaa.gov). All the figures are plotted using GrADS.

**REFERENCES:**


[1] JOSHI M, HAWKINS E, SUTTON R, et al. Projections of when temperature change will exceed 2° C above pre-industrial levels [J]. Nature: Climate Change, 2011, 1 (8): 407-412.

[2] ZHANG X D, LU C H, GUAN Z Y. Weakened cyclones, intensified anticyclones and recent extreme cold winter weather events in Eurasia [J]. Environ Res Lett, 2012, 7, 044044, doi: 10.1088/1748-9326/7/4/044044.

[3] DOMINGUES C M, CHURCH J A,WHITE N J, et al. Improved estimates of upper-ocean warming and muti-decadal sea-level rise [J]. Nature, 2008, 453(7 198): 1090-1093.

[4] IPCC. Climate change: The physical science basis [M]. Cambridge: Cambridge University Press, 2007: 996.

[5] CHAHINE M T. The hydrological cycle and its influence on climate [J]. Nature, 1992, 359(6 394): 373-380.

[6] SOROOCHIAN S, LAWFORD R G, TRY P, et al. Water and energy cycles: investigating the links [J]. WMO Bull, 2005, 54(2): 58-64.

[7] CHRISTY J R, TRENBERTH K E, ANDERSON J R. Large- scale redistributions of atmospheric mass [J]. J Climate, 1989, 2(2): 137-148.

[8] KUSUNOKI S, YOSHIMURA J, YOSHIMURA H, et al. Change of Baiu rain band in global warming projection by an atmospheric general circulation model with a 20-km grid size [J]. J Meteor Soc Japan, 2006, 84(4): 581-611.

[9] GIORGI F. Simulation of regional climate using a limited area model nested in a general circulation model [J]. J Climate, 1990, 3(8): 941-963.

[10] THOMPSON S L, POLLARD D. A global climate model with a land surface transfer scheme, Part I: present climate simulation [J]. J Climate, 1995, 8(4): 732-761.

[11] CHEN Ming, FU Cong-bin. A nest procedure between regional and global climate model and its application in long term climate simulations [J]. Chin J Atmos Sci, 2000, 24(2): 253-262.

[12] JU Li-xia, WANG Hui-jun. Modern climate over East Asia simulated by a regional climate model nested in a global grid point general circulation model [J]. Chin J Geophys, 2006, 49(1): 52-60.

[13] FINDLATER J. A major low-level air current near the Indian Ocean during the northern summer [J]. Quart J Roy Meteor Soc, 1969, 95(404): 362-380.

[14] CARLETON A M. Synoptic interaction between Antarctica and lower latitudes [J]. Aust Meteor Mag, 1992, 40(3): 129-147.

[15] ZENG Qing-cun, LI Jian-ping. Interactions between the Northern and Southern Hemispheric atmospheres and the essence of monsoon [J]. Chin J Atmos Sci, 2002, 26 (4): 433-448.

[16] WALLACE J M. North Atlantic oscillation annual mode: two paradigms-one phenomenon [J]. Quart J Roy Meteor Soc, 2000, 126(564): 791-805.

[17] WATANABE M. Asian jet waveguide and a downstream extension of the North Atlantic Oscillation [J]. J Climate, 2004, 17(24): 4674-4691.

[18] MANTUA N J, HARE S R, ZHANG Y, et al. A Pacific interdecadal climate oscillation with impacts on salmon production [J]. Bull Amer Meteor Soc, 1997, 78 (6): 1069-1079.

[19] THOMPSON D W J, WALLACE J M. The Arctic oscillation signature in the wintertime geopotential height and temperature fields [J]. Geophys Res Lett, 1998, 25 (9): 1297-1300.

[20] GONG D Y, WANG S W. Definition of Antarctic oscillation index [J]. Geophys Res Lett, 1999, 26 (4): 459-462.

[21] WALLACE J M, GUTZLER D S. Teleconnections in the geopotential height field during the North Hemisphere winter [J]. Mon Wea Rev, 1981, 109(4): 784-812.

[22] HOSKINS B J, JAMES I N, WHITE G H. The shape, propagation and mean-flow interaction of large-scale weather systems [J]. J Atmos Sci, 1983, 40 (7): 1595-1612.

[23] SHI N, ZHU Q G. Studies on the Northern early summer teleconnection patterns, their interannual variations and relation to drought/flood in China [J]. Adv Atmos Sci, 1993, 10(2): 155-168.

[24] CAO Lu, SUN Zheng-hu, REN Fu-min, et al. Study of a comprehensive monitoring index for two types of ENSO events [J]. J Trop Meteor, 2013, 29(1): 66-74.

[25] LIU Zheng-qi, LIU Yu-guo, HA Yao, et al. Role of equatorial Pacific Ocean subsurface oceanic temperature mode in ENSO cycle [J]. J Trop Meteor, 2013, 29(2): 255-261.

[26] GUAN Z Y, YAMAGATA T. Interhermispheric oscillations in the surface air pressure field [J]. Geophys Res Lett, 2001, 28(2): 263-266.

[27] WANG Ji-zhi, LI Mai-cun. Cross-equator flow from Australia and monsoon over China [J]. Chin J Atmos Sci, 1982, 6(1): 1-10.

[28] KALNAY E, KANAMITSU M, KISTLER R, et al. The NCEP-NCAR 40-year reanalysis project [J]. Bull Amer Meteor Soc, 1996, 77(3): 437-471.

[29] XIE P, ARKIN P A. Global precipitation：A17 year monthly analysis based on gauge observation, satellite estimates, and numerical model outputs [J]. Bull Amer Meteor Soc, 1997, 78(11): 2539-2558.

[30] THOMPSON D W J, WALLACE J M. Annular modes in the extratropical circulation. Part I: Month-to-month variability [J]. J Climate, 2000, 13(5): 1000-1016.

[31] MCPHADEN M J, LEE T, MCCLURG D. El Niño and its relationship to changing background conditions in the tropical Pacific Ocean [J]. Geophys Res Lett, 2011, 38, L15709, doi: 10.1029/2011GL048275.

[32] MCPHADEN M J. A 21st century shift in the relationship between ENSO SST and warm water volume anomalies [J]. Geophys Res Lett, 2012, 39, L09706, doi: 10.1029/2012GL051826.

[33] WU Guo-xiong, MENG Wen. Gearing between the Indo-monsoon circulation and the Pacific-Walker circulation and the ENSO. Part I: data analyses [J]. Chin J Atmos Sci, 1998, 22 (4): 470-480.

[34] ALEXANDER M, SCOTT J, BLADE I, et al. Extratropical air-sea interaction during ENSO: Atmospheric forcing and oceanic feedbacks [C]//11th conference on interaction of the sea and atmosphere, San Diego, 2001: 84-87.

[35] SUAREZ M J, SCHOPF P S. A delayed action oscillator for ENSO [J]. J Atmos Sci, 1988, 45(21): 3283-3287.

[36] JIN F F. An equatorial ocean recharge paradigm for

ENSO, Part I: conceptual Model [J]. J Atmos Sci, 1997, 54(7): 811-829.
[37] GILL A E. Some simple solution for heat-induced tropical circulation [J]. Quart J Roy Meteor Soc, 1980, 106(5): 447-462.
[38] WANG B, LIU J, KIM H J, et al. Northern Hemisphere summer monsoon intensified by mega-El Niño/southern oscillation and Atlantic multidecadal oscillation [J]. PNAS, 2013, 110(14): 5347-5352.
[39]HOSKINS B J, KAROLY D J. The steady linear response of a spherical atmosphere to thermal and orographic forcing [J]. J Atmos Sci, 1981, 38(6): 1179-1196.
[40] GONG Dao-yi, WANG Shao-wu. Impact of ENSO on rainfall of global land and China [J]. Chin Sci Bull, 1999, 44(9): 852-857.
[41] LU Chu-han, HUANG Lu, HE Jin-hai, et al. Interannual variability of heat content in western pacific warm pool and its impact on the eastern Asian climatic anomaly [J]. J Trop Meteor, 2014, 30(1): 64-72.
[42] HUANG Rong-hui, SUN Feng-ying. Impacts of the thermal state and the convective activities in the tropical western warm pool on the summer climate anomalies in East Asia [J]. Chin J Atmos Sci, 1994, 18(2): 141-151.
[43] KILADIS G N , DIAZ H F. Global climate anomalies associated with extremes in the Southern Oscillation [J]. J Climate, 1989, 2(9): 1069-1090.

**Citation:** TANG Wei-ya, GUAN Zhao-yong and QIAN Dai-li. A principal mode of circulation covariation between the Northern and Southern Hemispheres and its association with ENSO during boreal winter [J]. J Trop Meteor, 2017, 23(4): 450-461.